nature nanotechnology

LETTERS

PUBLISHED ONLINE: 9 AUGUST 2009 | DOI: 10.1038/NNANO.2009.195

A quantitative fluorescence study of protein monolayer formation on colloidal nanoparticles

Carlheinz Röcker[1], Matthias Pötzl[1], Feng Zhang[2], Wolfgang J. Parak[2] and G. Ulrich Nienhaus[1,3,4]*

It is now known that nanoparticles, when exposed to biological fluid, become coated with proteins and other biomolecules to form a 'protein corona'[1]. Recent systematic studies have identified various proteins that can make up this corona, but these nanoparticle–protein interactions are still poorly understood, and quantitative studies to characterize them are few in number. Here, we have quantitatively analysed the adsorption of human serum albumin onto small (10–20 nm in diameter) polymer-coated FePt and CdSe/ZnS nanoparticles by using fluorescence correlation spectroscopy. The protein corona forms a monolayer with a thickness of 3.3 nm. Proteins bind to the negatively charged nanoparticles with micromolar affinity, and time-resolved fluorescence quenching experiments show that they reside on the particle for ~100 s. These new findings deepen our quantitative understanding of the protein corona, which is of utmost importance in the safe application of nanoscale objects in living organisms.

Colloidal inorganic nanoparticles can be synthesized in structurally highly defined ways from many different materials[2,3]. An organic ligand shell surrounding the inorganic nanoparticle cores, which endows them with colloidal stability, can also be prepared in a highly ordered fashion[4]. Adsorption of proteins to the surface of such nanoparticles has been reported in several studies, but quantitative studies of nanoparticle–protein interactions are still scarce[1]. Because the interaction of nanoparticles with biological matter, including cellular uptake, depends on their surface properties, detailed studies of the biological coating of nanoparticles are required so that their potential can be fully exploited while avoiding possible safety risks[5].

To investigate protein adsorption to highly defined, small nanoparticles, we chose crystalline FePt (ref. 6) and CdSe/ZnS (ref. 7) nanocrystals embedded in an amphiphilic polymer[8]. The polymer coatings of the FePt and CdSe/ZnS nanoparticles contain carboxyl groups and are negatively charged[9]. An organic fluorophore (DY-636) was introduced into the polymer shell of the FePt particles to render them fluorescent[10]; the CdSe/ZnS quantum dots are autofluorescent[11]. As a model protein we selected human serum albumin (HSA), a major soluble constituent of human blood plasma and thus a relevant target for studies of nanoparticle–protein interactions. The polypeptide chain of HSA is folded into a three-domain structure with an overall heart-shaped conformation (Fig. 1a) that can be approximated by an equilateral triangular prism, with sides of ~8 nm and a height of ~3 nm (Fig. 1b)[12].

To quantitatively monitor HSA adsorption onto the fluorescent nanoparticles, we used fluorescence correlation spectroscopy (FCS), a technique that measures fluorescence bursts emitted by particles diffusing through a small observation volume ($\sim 1 \times 10^{-15}$ l), which is formed by tight focusing of a laser spot[13–16]. Autocorrelation analysis of the fluorescence emission

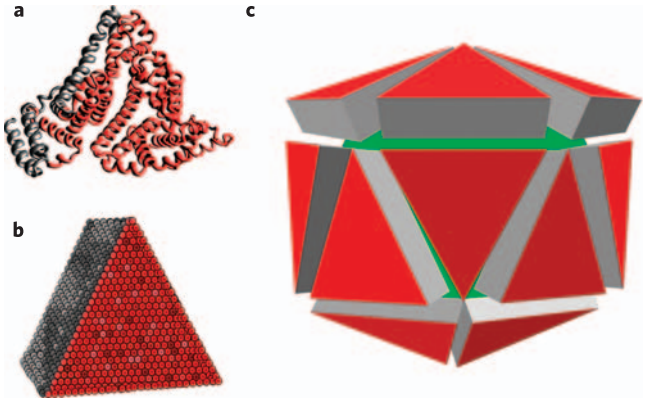

Figure 1 | Structure of HSA and the protein corona. a,b, Representation of the HSA polypeptide chain (**a**), which can be approximated by an equilateral triangular prism (**b**). **c**, At concentrations of HSA typically found in serum, the surface of the polymer-coated FePt nanoparticles (green) is covered by a monolayer of about 20 HSA molecules (red triangular prisms).

time traces yields a characteristic timescale of diffusion τ_D, from which the diffusion coefficient D and, by means of the Stokes–Einstein relation, the hydrodynamic radius R_H can be extracted. Thus, we can directly observe the increasing nanoparticle size due to protein binding to its surface. Only nanomolar concentrations of the particles in microlitre-sized volumes are needed for FCS, whereas other methods for size determination such as dynamic light scattering or gel permeation chromatography require large amounts of samples.

The size of the bare, DY-636-labelled FePt nanoparticles was determined from the autocorrelation function (Fig. 2) as $R_H(0) = 5.6 \pm 0.2$ nm, which agrees well with estimates from gel electrophoresis (see Supplementary Information). This parameter was fixed in the subsequent analysis of protein binding equilibria. FCS autocorrelation curves were measured for 4 nM nanoparticle solutions containing HSA concentrations ranging from 60 nM to 1 mM (Fig. 2). The resultant (average) R_H values increase with higher protein concentration in a stepwise fashion (Fig. 3), revealing a limited loading capacity of the nanoparticles. Saturation was reached at physiological concentrations of HSA in human blood plasma (500–800 μM). We describe the dependence on the number N of bound proteins, $R_H(N)$, by the expression (see Supplementary Information for details)

$$R_H(N) = R_H(0)\sqrt[3]{(1 + cN)} \qquad (1)$$

where c is a scaling factor and N represents the average number of protein molecules bound to the nanoparticles at a

[1]Institute of Biophysics, University of Ulm, Albert Einstein-Allee 11, 89081 Ulm, Germany, [2]Fachbereich Physik, Philipps Universität Marburg, Renthof 7, 35037 Marburg, Germany, [3]Institute of Applied Physics and Center for Functional Nanostructures, University of Karlsruhe (TH), 76128 Karlsruhe, Germany, [4]Department of Physics, University of Illinois at Urbana-Champaign, Urbana, Illinois 61801, USA. *e-mail: uli@uiuc.edu

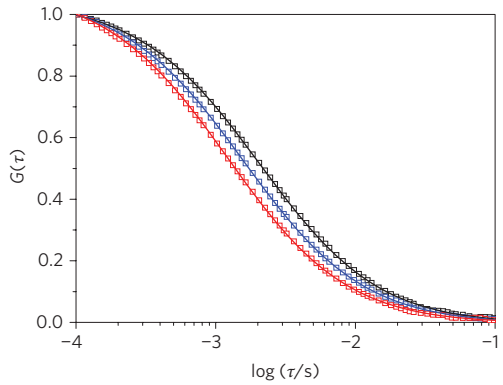

Figure 2 | Examples of FCS autocorrelation functions of polymer-coated FePt nanoparticles in the absence and presence of HSA. The correlation curves measured with 4 μM HSA (blue squares) and 500 μM HSA (black squares) in the solution are shifted toward longer times compared to the pure nanoparticles (red squares). The best-fit model curves are shown as solid lines.

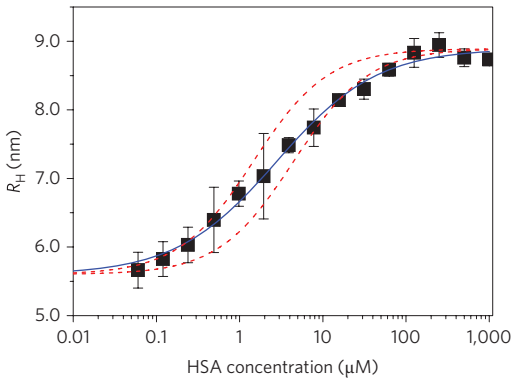

Figure 3 | Association of HSA to polymer-coated FePt nanoparticles measured by FCS. The hydrodynamic radii of the particles are plotted as a function of HSA concentration. The data points are averages from three independent series of measurements. The blue solid line represents a fit of an anti-cooperative binding model (equations (1) and (2)) to the data, and the red dashed lines are Langmuir binding isotherms fitted to the first and last 20% of the transition.

specific HSA concentration in the solution. Thus, at saturation, $R_H(N_{max}) = R_H(0) + \Delta R = R_H(0)\sqrt[3]{(1 + cN_{max})}$. The dependence of N on the protein concentration [HSA] is modelled by

$$N = N_{max}\frac{1}{1 + (K'_D/[HSA])^n} \quad (2)$$

where N_{max} is the maximum number of proteins binding to the nanoparticle, n is the Hill coefficient, and K'_D is the dissociation coefficient, which quantifies the strength of the protein–nanoparticle interaction. An excellent fit of the data is achieved with this model (Fig. 3), yielding $K'_D = 5.1 \pm 1.3$ μM, and an increase of R_H by $\Delta R = 3.3 \pm 0.3$ nm at saturation. The Hill coefficient ($n = 0.74 \pm 0.1$), being markedly below one, indicates anti-cooperative binding. Langmuir isotherms (non-cooperative binding, $n = 1$) are also plotted in Fig. 3; they are steeper and suggest an affinity change by a factor of ~3 across the transition. The anti-cooperativity may arise from steric hindrance, which imposes an energetic penalty on proteins binding to a partially coated nanoparticle.

Recent hydrodynamic studies have confirmed the equilateral triangular prism model shape from the X-ray structure[12] for (bovine) serum albumin in solution, using triangular sides of 8.4 nm and a thickness of 3.15 nm (ref. 17). (The larger dimensions are expected due to the associated hydration water layer.) Consequently, the increase of the nanoparticle radius of 3.3 nm measured by FCS suggests that HSA molecules form a monolayer around the nanoparticles, covering the surface with their large triangular faces. The saturation behaviour clearly proves that protein association beyond the first layer is negligible. For complete surface coverage, there is room for about 20 HSA molecules on each FePt nanoparticle, as estimated from the surface area of a sphere with radius $R_0 + \Delta R/2$.

For carboxylic acid-functionalized quantum dots, analogous FCS experiments yielded a hydrodynamic radius $R_H(0) = 7.9 \pm 0.3$ nm for the bare quantum dots. Exposure to HSA solutions showed a similar saturation behaviour, with a radius increase of $\Delta R = 3.2 \pm 0.4$ nm, which again indicates a single protein layer. (The data are shown in the Supplementary Information.) Likewise, an anti-cooperative binding isotherm, with $n = 0.78 \pm 0.15$, was observed. The dissociation coefficient, $K'_D = 37 \pm 12$ μM, however, was almost an order of magnitude larger, reflecting a markedly weaker interaction between HSA and the quantum dot surface.

These equilibrium binding studies were complemented by kinetic experiments to assess the temporal behaviour of the association and dissociation processes. To this end, we used time-resolved fluorescence quenching to monitor the association of protein molecules labelled with a dye moiety that quenches the emission of the DY-636-labelled FePt nanoparticles. In Fig. 4a, normalized fluorescence kinetics traces are plotted at four different concentrations of QSY 21-labelled HSA. As expected, HSA binding speeds up with increasing protein concentration. The kinetics are non-exponential but can be fitted by stretched exponential functions[18] as simple representations of rate distributions,

$$I(t) = I_0 \exp(-(t/\tau)^\beta) \quad (3)$$

which are governed by the characteristic time constant τ and the stretching exponent β ($0 < \beta < 1$). The latter parameter controls the width of the corresponding rate distribution. With increasing protein concentrations, the fits typically yielded a decrease in τ and β (see Supplementary Table S1). A mean relaxation time $\langle\tau\rangle$ can be calculated using

$$\langle\tau\rangle = \frac{\tau}{\beta}\Gamma(\beta^{-1}) \quad (4)$$

where Γ denotes the gamma function. The associated relaxation rate, $\lambda = \langle\tau\rangle^{-1}$, increases linearly with HSA concentration within error (Fig. 4b). Assuming a simple bimolecular reaction under pseudo first-order conditions, the apparent rate coefficient λ is given by

$$\lambda = \langle\tau\rangle^{-1} = \langle k_{off}\rangle + \langle k_{on}\rangle \cdot [\mathrm{HSA}] \quad (5)$$

The intercept and slope of the line yield the average backward and forward rate coefficients for protein association, $\langle k_{off}\rangle = (9 \pm 2) \times 10^{-3}\ s^{-1}$ and $\langle k_{on}\rangle = (2.4 \pm 0.5) \times 10^3\ M^{-1}\ s^{-1}$, respectively. Consequently, the mean residence time of HSA on the nanoparticle surface is $\langle k_{off}\rangle^{-1} \approx 100$ s. The average rate coefficient for the association process is about five orders of magnitude below typical estimates for diffusion-controlled protein reactions ($k_{on} \approx 1 \times 10^8\ M^{-1}\ s^{-1}$). Thus, a large number of encounters precede a successful HSA binding event. This behaviour may indicate that both the protein and nanoparticle surface have to adapt their structures to form a stable interface. At high protein coverage of the nanoparticle surface, one could also envision that rearrangements of protein molecules already bound to the nanoparticle are required to make room for an incoming protein molecule. This crowding

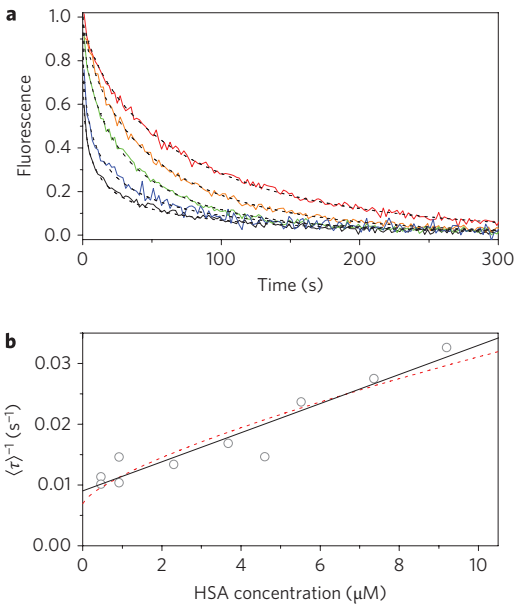

Figure 4 | Kinetic studies of HSA association to polymer-coated FePt nanoparticles. a, Kinetic traces of fluorescence quenching are shown for five different concentrations (red, 0.5 μM; orange, 4 μM; green, 6 μM; blue, 8 μM; black, 10 μM) of QSY 21-labelled HSA (solid lines) together with stretched exponential model functions (dashed lines). **b**, Concentration dependence of the average relaxation rate and the best fit using linear ($\propto$ [HSA], black solid line) and sublinear ($\propto$ [HSA]$^{0.74}$, red dashed line) relations.

effect is expected to lower the on rates (and possibly increase the off rates) and may contribute significantly to the observed dispersion of the apparent rates (Fig. 4a).

Taking the ratio $\langle k_{off}\rangle/\langle k_{on}\rangle$, we can compute an average equilibrium dissociation coefficient $K_D \approx 3.8 \pm 1.5$ μM for the protein–nanoparticle interaction, which is in excellent agreement with the value of 5.1 ± 1.3 μM obtained from the FCS measurement. Although this result is satisfying, we note that this treatment is rather simplistic for an anti-cooperative reaction as observed in the equilibrium experiments. Indeed, $n = 0.74$ would imply a sub-linear behaviour, shown by the dashed line in Fig. 4b. The non-exponential kinetics imply a more complex reaction scheme, as already discussed above, that cannot be adequately captured by average rate coefficients.

HSA forms a protein monolayer on the surface of small, carboxy-functionalized nanoparticles, as shown here by FCS experiments. HSA binding occurs with micromolar affinity and an anti-cooperative binding isotherm. Time-resolved fluorescence quenching experiments reveal non-exponential kinetics and average rate coefficients for HSA association and dissociation; the results are in excellent agreement with the FCS equilibrium data. The techniques used here allow the precise determination of the essential kinetic, equilibrium and structural parameters of protein binding to nanoparticles, using only microlitre volumes of nanomolar nanoparticle solutions. We will extend these studies to other relevant proteins[19] and nanoparticles with specifically tailored surface properties, including competition assays, with the aim to further our understanding of protein–nanoparticle interaction at the molecular level.

Methods

Nanoparticles. FePt nanoparticle cores were synthesized following a previously published protocol[6]. To render them water soluble, they were coated with an amphiphilic polymer synthesized from dodecylamine and poly(isobutylene-alt-maleic anhydride) that was labelled with the amino-modified fluorescent dye DY-636 (Dyomics). These nanoparticles, which carry carboxylic acid groups on their surfaces to endow them with colloidal stability, are interesting bifunctional, both optical and magnetic probes for biomedical imaging. A detailed description of the synthesis is provided in the Supplementary Information. For comparative studies, CdSe/ZnS quantum dots functionalized with a similar amphiphilic polymer with carboxylic acid groups (Qdot ITK 655) were purchased from Invitrogen. The surface composition of these commercial nanoparticles is not precisely specified, however.

Fluorescence correlation spectroscopy. FCS experiments were performed on a home-built confocal microscope similar to those described previously[20,21]. The instrument design was based on an inverted epifluoresence microscope (Axiovert 200, Carl Zeiss). The 635-nm excitation light from a diode laser (Chromalase 635, Blue Sky Research) was delivered to the back port of the microscope by a single-mode optical fibre (QSMJ, OZ Optics). The emitted light was collected by a water immersion objective (UPLAPO 60×/1.2w, Olympus), passed through a dichroic mirror (z532/633xr, AHF) and a band-pass filter (HQ 690/80, AHF), and focused onto a 62.5-μm-diameter gradient index fibre (Thorlabs), which replaced the confocal pinhole. The fluorescence signal was detected by an avalanche photodiode (SPCM-CD3017, Perkin Elmer) and processed by a digital correlator (ALV-5000/E, ALV). All measurements were performed in a temperature-controlled laboratory at 22 °C using an excitation power of 6 μW.

FCS measurements were performed in PBS buffer (Dulbecco's PBS without Ca^{2+} and Mg^{2+}, PAA Labs). Gel filtration cartridges (Edge BioSystems) and centrifugation filters (100 kDa, Pall Nanosep) were used for buffer exchange and removal of aggregates, respectively. For FCS binding measurements, ~4 nM nanoparticle solutions with varying concentrations of HSA (Sigma-Aldrich) were prepared by mixing equal volumes of the corresponding stock solutions. Sample solutions were kept between two standard cover slips separated by 200-μm mylar foils, leaving a 3-mm-wide channel for the sample solution in the middle. They were sequentially exchanged in order of increasing protein concentration during one measurement series. The stability of the setup was checked by control measurements at the beginning and the end of each series with a calibration sample, using 3 nM ATTO 655 (ATTO-TEC) in water at 22 °C as a standard. Its diffusion coefficient, 3.93×10^{-10} m^2 s^{-1}, was calculated from the value measured by two-focus FCS measurements[22] at 25 °C by rescaling to 22 °C with the known temperature dependence of the water viscosity. The FCS experiment was very sensitive to the presence of large aggregates, and therefore, 5−15 independent autocorrelation functions were measured (60 s each) and averaged; data sets affected by aggregates were excluded. (Additional remarks on nanoparticle studies by FCS are included as Supplementary Information.) Autocorrelation functions $G(\tau)$ were analysed by custom-written software, using a one-species, three-dimensional diffusion model with an additional exponential reaction term,

$$G(\tau) = \frac{1}{\langle N\rangle}\left(1+\frac{\tau}{\tau_D}\right)^{-1}\left(1+\left(\frac{r_0}{z_0}\right)^2\frac{\tau}{\tau_D}\right)^{-\frac{1}{2}}\cdot\left(1+Ae^{-k_R\tau}\right) \qquad (6)$$

where $\langle N\rangle$ denotes the average number of particles in the observation volume of three-dimensional Gaussian shape, with radial extension r_0 and axial extension z_0. The diffusion time τ_D is related to the translational diffusion coefficient of the particles, $D = r_0^2/4\tau_D$. The exponential term accounts for the photodynamics of the dye on fast timescales, and its parameters, A and k_R, were included for a proper fit of the autocorrelation function but are not of relevance here. From the resulting diffusion coefficients, hydrodynamic radii were calculated according to the Stokes–Einstein relation, $R_H = kT/6\pi\eta D$. Statistical errors are specified as standard deviations in the text; systematic errors introduced by FCS modelling and analysis are estimated to contribute with <5% of the absolute R_H values. Changes in viscosity due to the increasing protein concentration were taken into account by using a linear approximation for the contribution of the solute to the solution viscosity based on the intrinsic viscosity of HSA of 4.2 cm^3 g^{-1}, as specified by the supplier (Sigma-Aldrich).

Fluorescence quenching kinetics. HSA was labelled with the amine-reactive fluorescence quencher QSY 21 succinimidyl ester (Invitrogen) at a ratio of 1:4, as determined by absorption spectroscopy. Kinetic fluorescence measurements were performed on a SPEX Fluorolog II (HORIBA Jobin Yvon) at 8.5-nm bandwidth for excitation (630 nm) and emission (660 nm) in PBS buffer. Solutions with a final particle concentration of ~4 nM and varying concentrations of quencher-labelled HSA were prepared by mixing equal volumes from stock solutions; the fluorescence signal was recorded with a time resolution of 0.2 s.

Received 17 March 2009; accepted 2 July 2009;
published online 9 August 2009

References

1. Cedervall, T. *et al.* Understanding the nanoparticle–protein corona using methods to quantify exchange rates and affinities of proteins for nanoparticles. *Proc. Natl Acad. Sci. USA* **104,** 2050–2055 (2007).
2. Scher, E. C., Manna, L. & Alivisatos, A. P. Shape control and applications of nanocrystals. *Phil. Trans. R. Soc. Lond. A* **361,** 241–257 (2002).

3. Kudera, S. *et al.* Synthesis and perspectives of complex crystaline nanostructures. *Phys. Stat. Sol.* (*a*) **203,** 1329–1336 (2006).
4. Jadzinsky, P. D., Calero, G., Ackerson, C. J., Bushnell, D. A. & Kornberg, R. D. Structure of a thiol monolayer-protected gold nanoparticle at 1.1 Å resolution. *Science* **318,** 430–433 (2007).
5. Colvin, V. L. The potential environmental impact of engineered nanomaterials. *Nature Biotechnol.* **21,** 1166–1170 (2003).
6. Sun, S., Murray, C. B., Weller, D., Folks, L. & Moser, A. Monodisperse FePt nanoparticles and ferromagnetic FePt nanocrystal superlattices. *Science* **287,** 1989–1992 (2000).
7. Dabbousi, B. O. *et al.* (CdSe)ZnS core−shell quantum dots: synthesis and characterization of a size series of highly luminescent nanocrystallites. *J. Phys. Chem. B* **101,** 9463–9475 (1997).
8. Pellegrino, T. *et al.* Hydrophobic nanocrystals coated with an amphiphilic polymer shell: a general route to water soluble nanocrystals. *Nano Lett.* **4,** 703–707 (2004).
9. Lin, C. A. *et al.* Design of an amphiphilic polymer for nanoparticle coating and functionalization. *Small* **4,** 334–341 (2008).
10. Fernandez-Arguelles, M. T. *et al.* Synthesis and characterization of polymer-coated quantum dots with integrated acceptor dyes as FRET-based nanoprobes. *Nano Lett.* **7,** 2613–2617 (2007).
11. Wu, X. *et al.* Immunofluorescent labeling of cancer marker Her2 and other cellular targets with semiconductor quantum dots. *Nature Biotechnol.* **21,** 41–46 (2003).
12. He, X. M. & Carter, D. C. Atomic structure and chemistry of human serum albumin. *Nature* **358,** 209–215 (1992).
13. Lamb, D. C., Schenk, A., Röcker, C., Scalfi-Happ, C. & Nienhaus, G. U. Sensitivity enhancement in fluorescence correlation spectroscopy of multiple species using time-gated detection. *Biophys. J.* **79,** 1129–1138 (2000).
14. Maiti, S., Haupts, U. & Webb, W. W. Fluorescence correlation spectroscopy: diagnostics for sparse molecules. *Proc. Natl Acad. Sci. USA* **94,** 11753–11757 (1997).
15. Rigler, R. & Elson, E. S. (eds) *Fluorescence Correlation Spectroscopy: Theory and Applications* (Springer, 2001).
16. Thompson, N. L. in *Topics in Fluorescence Spectroscopy* Vol. 1 (ed. Lakowicz, J. R.) 337–378 (Plenum Press, 1991).
17. Ferrer, M. L., Duchowicz, R., Carrasco, B., de la Torre, J. G. & Acuna, A. U. The conformation of serum albumin in solution: a combined phosphorescence depolarization-hydrodynamic modeling study. *Biophys. J.* **80,** 2422–2430 (2001).
18. Kohlrausch, R. Theorie des elektrischen Rueckstandes der Leidner Flasche. *Pogg. Ann. Phys. Chem.* **91,** 56–82 (1854).
19. Cedervall, T. *et al.* Detailed identification of plasma proteins adsorbed on copolymer nanoparticles. *Angew Chem. Int. Ed.* **46,** 5754–5756 (2007).
20. Schenk, A., Ivanchenko, S., Röcker, C., Wiedenmann, J. & Nienhaus, G. U. Photodynamics of red fluorescent proteins studied by fluorescence correlation spectroscopy. *Biophys. J.* **86,** 384–394 (2004).
21. Wiedenmann, J. *et al.* EosFP, a fluorescent marker protein with UV-inducible green-to-red fluorescence conversion. *Proc. Natl Acad. Sci. USA* **101,** 15905–15910 (2004).
22. Dertinger, T. *et al.* Two-focus fluorescence correlation spectroscopy: a new tool for accurate and absolute diffusion measurements. *ChemPhysChem* **8,** 433–443 (2007).

Acknowledgements

This work was supported by the Deutsche Forschungsgemeinschaft (DFG) through the Center for Functional Nanostructures (CFN) and Schwerpunktprogramm (SPP) 1313, grants NI291/7 and PA794/4.

Author contributions

C.R. and G.U.N. conceived and designed the experiments. C.R. and M.P. performed the experiments. C.R. and M.P. analysed the data. F.Z. and W.P. contributed materials. C.R., W.P. and G.U.N. co-wrote the paper. All authors discussed the results and commented on the manuscript.

Additional information

Supplementary information accompanies this paper at www.nature.com/naturenanotechnology. Reprints and permission information is available online at http://npg.nature.com/reprintsandpermissions/. Correspondence and requests for materials should be addressed to G.U.N.